Supporting Information for "Observations of near-surface current shear help describe oceanic oil and plastic transport"

Nathan J.M. Laxague,[1] Tamay M. Özgökmen,[2] Brian K. Haus,[2], Guillaume Novelli,[2] Andrey Shcherbina,[3] Peter Sutherland,[4] Cédric M. Guigand,[2] Björn Lund,[2] Sanchit Mehta,[2] Matías Alday,[4] and Jeroen Molemaker[5]

[1]Department of Ocean and Climate Physics, Lamont-Doherty Earth Observatory, Columbia University, Palisades, NY, USA
[2]Department of Ocean Sciences, Rosenstiel School of Marine and Atmospheric Science, University of Miami, Miami, FL, USA
[3]Applied Physics Laboratory, University of Washington, Seattle, WA, USA
[4]Laboratoire d'Oceanographie Physique et Spatiale, L'Institut Francais de Recherche pour l'Exploitation de la Mer, Centre Bretagne, Plouzané, FR
[5]University of California Los Angeles, Atmospheric and Oceanic Sciences, Los Angeles, CA, USA

Corresponding author: Nathan J.M. Laxague, `laxague@ldeo.columbia.edu`

Contents of this file

Introduction

The text that follows describes each type of sensor used in acquiring the data shown in the main manuscript. The figures provide additional information which may be useful to the reader.

Text S1 - Polarimetric Camera

A bow tower-mounted polarimetric camera was used to measure the spatiotemporal development of the short wave slope field [*Zappa et al.*, 2008], taking into account the vessel's rotational [*Laxague et al.*, 2015] and translational [*Laxague et al.*, 2017] motion. Each ten seconds of sea surface slope fields were packaged into a 780x780x200 array and subjected to a 3D Fourier transform, producing a wavenumber-frequency spectrum; these were averaged over the sampling duration of four hours. Wavenumbers ranged from 5-1500 rad/m; frequencies ranged from 0.1-10 Hz. Bound waves [*Plant et al.*, 1999] were identified and removed from the spectra. Once this operation had been performed, departures from the gravity-capillary linear dispersion relation were logged at each wavenumber component and used to estimate current [*Laxague et al.*, 2017], with depth taken from literature [*Plant and Wright*, 1980] as 4.4% of the wavelength. All measured velocity profiles were arranged to yield a profile (and the 5^{th}-95^{th}-percentile range) that was bin-averaged in the vertical to produce layer thicknesses of 1 mm (as shown in main document Figure 2).

Text S2 - Drifting Instruments

The GPS-tracked drifters ("CARTHE" drifters- `http://www.greenwaveinstruments.com`) were specifically developed with goals of being lower cost, easier to handle, and more biodegradable than previous designs- all while still accurately following the near-surface Lagrangian velocity. Each drifter body was constructed from injection-molded bio-plastic (PHA), biodegradable in seawater, and low-toxicity electronics for data transmission. A single drifter combines a surface float (containing the GPS transmitter and batteries) and a submerged drogue (draft of 70 cm, center of drag at 30 cm) connected by a chain tether that flexes to allow the drifter to more accurately follow the slope of the waves at the surface. Its drifting characteristics were extensively quantified in a wind-wave tank and in the field [*Novelli et al.*, 2017]. Measurements show that the drifter (respectively the floater alone) follows the average Lagrangian current, including wave Stokes drift, in the upper 0.65 m (respectively 0.035 m), to an accuracy better than 0.5% (respectively 2%) of the equivalent 10 m neutral wind speed U_{10}, over a range of 8-23 m/s. In field trials with U_{10} of 5-15 m/s, the velocities of CARTHE drifters matched that of neighboring CODE drifters to within 0.1% of U_{10}. Biodegradable bamboo dinner plates were deployed via small boat and tracked to measure near-surface currents. Each plate had a draft of 0.015 m and a diameter of 0.28 m, floating just below the surface. Given typical dry and wet bamboo densities of 860 kg/m^3 and 1160 kg/m^3, respectively [*Amada and Lakes*, 1997]- and that the nearest-surface water density during sampling time was ≈1140 kg/m^3, we estimate that the damp plates were at least 95% submerged, exposing a negligible amount to direct wind forcing. Tracking was performed on images recorded using a gimballed high-resolution (20 Megapixels) camera attached to a commercial UAV (drone). Each frame was georeferenced using the drone's GPS, altitude, and camera attitude records. At an altitude of 130 m, each plate was represented by approximately 10x10 pixels. In order to minimize the effect of error introduced into the current measurements from uncertainties in the GPS record (e.g., as described in [*Miyao and Isobe*, 2016]), the leading edge of the bamboo plates was tracked at the beginning and end of each drone flight. This ensured that the ≈5 meter total error in drone position between the two frames was diluted by a horizontal scale of ≈500 meters, or ≈1% error. This single drift speed was found to be within 2-3% of the drift speed computed from consecutive UAV frames, indicating that GPS error from one drone position to the next did not appreciably contaminate the current estimates.

Text S3 - ADCPs

Currents in the upper 5m of the water column were measured by a REMUS-100 Autonomous Underwater Vehicle (AUV) deployed concurrently with the drifter and plate release experiment. For the most of its mission, the AUV navigated at 2m depth along the parallel lines underneath the drifter field, with occasional dives to 10m to sample vertical stratification. The vehicle was equipped with upward- and downward-looking 1200kHz RDI ADCP. For the experiment, the ADCP was operated in the pulse-coherent mode, with the vertical bin resolution of 7 cm over the range of ±2.1 m above and below the vehicle (except for the ±0.4m blanking distance gap in the middle). Velocity measurements were referenced to the bottom, tracked continuously using dedicated ADCP pings. ADCP sampling rate was on the order of 0.65 Hz. Estimated RMS single-ping accuracy of velocity measurements was 1.8 cm/s. 80-minute average current profile spanning depth range from 0.2 to 4.4 m was used in the study (Fig. 2), with an estimated standard error of <2 cm/s attributable to wave orbital motions with the amplitude of up to 20 cm/s near the surface. Currents below 4 m were measured with the pole-mounted 1200kHz RDI ADCP on the R/V F. G. Walton Smith. The instrument was positioned in a downward-looking orientation at 3.25 m depth with a 50 cm blanking distance. Measurements spanned the range from 4 m to 1 m off the bottom, with 50 cm vertical bin spacing. Velocities were processed using the UHDAS system [*Firing et al.*, 2012], referenced to the bottom (correcting for ship translation) and time-averaged over the duration of the experiment.

Text S4 - Wind, Waves, Stokes Drift, and Water Density

The wind velocity vector was recorded at 20 Hz from a tower-mounted Campbell Scientific IRGASON sonic anemometer. Water surface elevation was recorded at 20 Hz from a bow-mounted pentagonal array of acoustic altimeters. With the aid of a six degree-of-freedom inertial motion unit, both sets of data were corrected for ship motion [*Anctil et al.*, 1994]. The wind stress vector (and through it, the friction velocity u_*) was computed from the corrected wind velocity time series via the eddy covariance method [*Edson et al.*, 2013]. The earth-referenced array of water surface elevation measurements were used to calculate the gravity wavenumber directional spectrum [*Donelan et al.*, 1996]. This was combined with the high-wavenumber spectrum computed from the polarimetric slope fields described above and converted into an intrinsic frequency directional spectrum (making sure to conserve energy [*Plant*, 2009] and further utilized to compute the directional Stokes Drift profile. The particular technique used for this computation ("2Dh-SD") accounts for the directional spreading of the wave field [*Webb and Fox-Kemper*, 2015]. The density profile shown in Figure 1c was computed using the International Equation of State for sea water (EOS-80) via temperature and salinity measurements obtained from a series of Castaway CTD profiles performed throughout the experiment.

References

Amada, S. and Lakes, R. S. (1997), Viscoelastic properties of bamboo, *Journal of Materials Science*, *32*, 2693-2697, doi:10.1023/A:1018683308211.

Anctil, F., M. A. Donelan, W. M. Drennan, and H. C. Graber (1994), Eddy-Correlation Measurements of Air-Sea Fluxes from a Discus Buoy, *Journal of Atmospheric and Oceanic Technology*, *11*(4), 7, doi:10.1175/1520-0426(1994)011<1144:ECMOAS>2.0.CO;2.

Donelan, M. A., W. M. Drennan, and A. K. Magnusson (1996), Nonstationary Analysis of the Directional Properties of Propagating Waves, *Journal of Physical Oceanography*, *26*(9), 1901–1914, doi:10.1175/1520-0485(1996)026<1901:NAOTDP>2.0.CO;2.

Edson, J. B., V. Jampana, R. a. Weller, S. P. Bigorre, A. J. Plueddemann, C. W. Fairall, S. D. Miller, L. Mahrt, D. Vickers, and H. Hersbach (2013), On the Exchange of Momentum over the Open Ocean, *Journal of Physical Oceanography*, *43*(8), 1589–1610, doi:10.1175/JPO-D-12-0173.1.

Firing, E., J. Hummon, and T. Chereskin (2012), Improving the Quality and Accessibility of Current Profile Measurements in the Southern Ocean, *Oceanography*, *25*(3), 164–165, doi:10.5670/oceanog.2012.91.

Laxague, N. J. M., B. K. Haus, D. Bogucki, and T. Özgökmen (2015), Spectral characterization of fine-scale wind waves using shipboard optical polarimetry, *Journal of Geophysical Research C: Oceans*, *120*(4), 3140–3156, doi:10.1002/2014JC010403.

Laxague, N. J. M., B. K. Haus, D. G. Ortiz-Suslow, C. J. Smith, G. Novelli, H. Dai, T. Özgökmen, H. C. Graber (2017), Passive Optical Sensing of the Near-Surface Wind-Driven Current Profile, *Journal of Atmospheric and Oceanic Technology*, *34*(5), 1097–1111, doi:10.1175/JTECH-D-16-0090.1.

Miyao, Y., and Isobe, A. (2016), A combined balloon photography and buoy-tracking experiment for mapping surface currents in coastal waters, *Journal of Atmospheric and Oceanic Technology*, *33* 1237-1250, doi:10.1175/JTECH-D-15-0113.1.

Novelli, G., C. Guigand, C. Cousin, E. Ryan, N. J. M. Laxague, H. Dai, B. K. Haus, and T. Ozgokmen (2017), A Biodegradable Surface Drifter For Ocean Sampling On A Massive Scale, *Journal of Atmospheric and Oceanic Technology*, doi:10.1175/JTECH-D-17-0055.1

Plant, W. J. (2009), The Ocean Wave Height Variance Spectrum: Wavenumber Peak versus Frequency Peak, *Journal of Physical Oceanography*, *39*(9), 2382–2383, doi:

10.1175/2009JPO4268.1.

Plant, W. J., and J. W. Wright (1980), Phase speeds of upwind and downwind traveling short gravity waves, *Journal of Geophysical Research*, *85*(C6), 3304, doi:10.1029/JC085iC06p03304.

Plant, W. J., W. C. Keller, V. Hesany, T. Kara, E. Bock, and M. A. Donelan (1999), Bound waves and Bragg scattering in a wind-wave tank, *Journal of Geophysical Research: Oceans*, *104*(C2), 3243–3263.

Webb, A., and B. Fox-Kemper (2015), Impacts of wave spreading and multidirectional waves on estimating Stokes drift, *Ocean Modelling*, *96*, 49–64, doi:10.1016/j.ocemod.2014.12.007.

Zappa, C. J., M. L. Banner, H. Schultz, A. Corrada-Emmanuel, L. B. Wolff, and J. Yalcin (2008), Retrieval of short ocean wave slope using polarimetric imaging, *Measurement Science and Technology*, *19*(5), 055,503, doi:10.1088/0957-0233/19/5/055503.

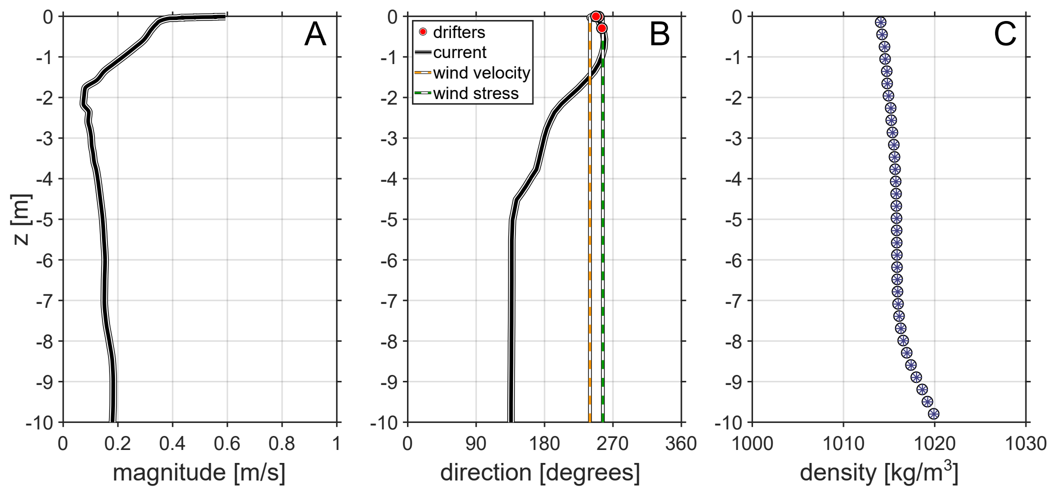

Figure 1. Current and density profile: Magnitude (a) and direction (b) of observed current, bearing of drifting instruments, and orientation of wind velocity & stress vectors. (c) Profile of water density obtained from the Castaway CTD profiler.

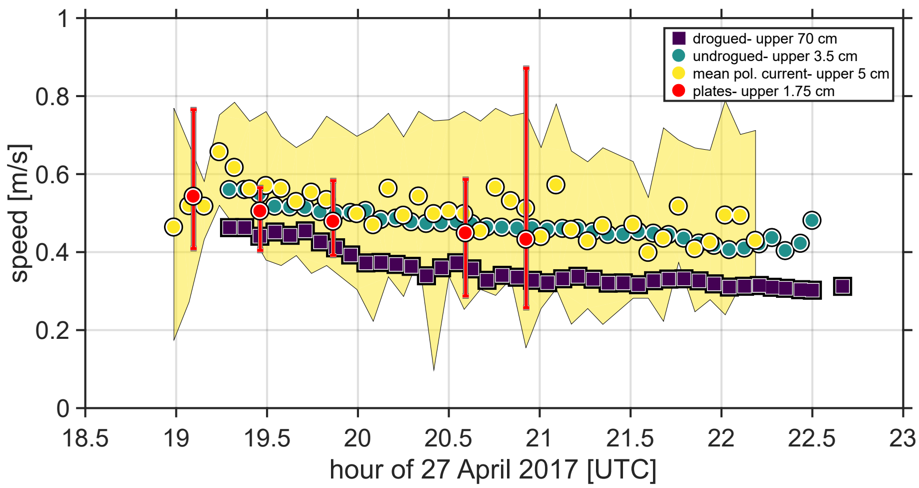

Figure 2. Current time series: Time series of drifter/plate centroid translation speeds and mean polarimetric camera-determined current magnitude. Yellow shaded region (red bars) represents 5th-95th percentile range for the camera-derived current magnitude (plate speed).

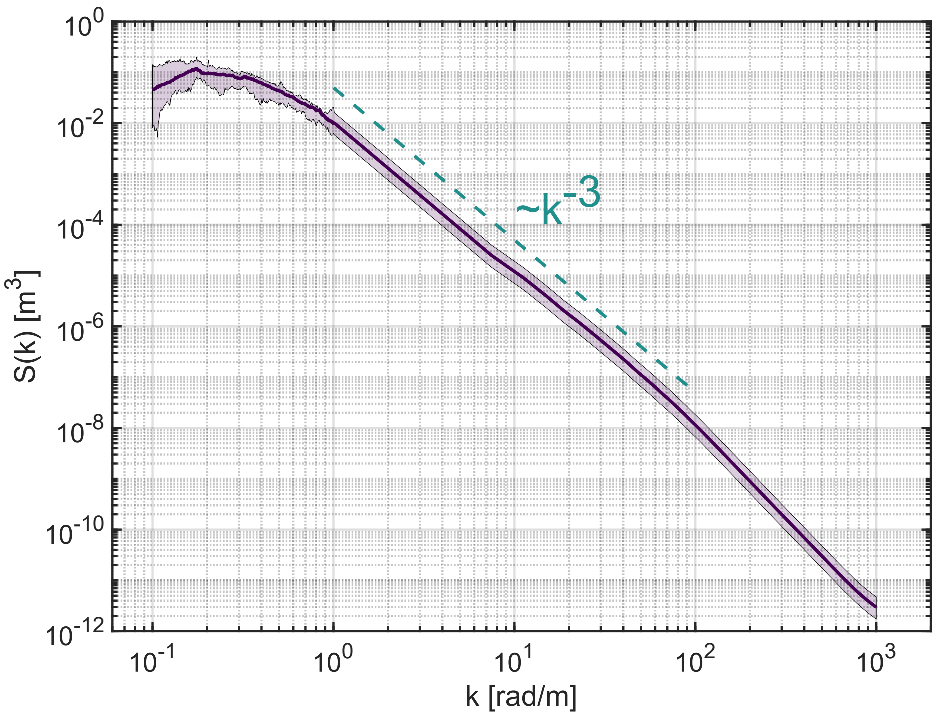

Figure 3. Composite spectrum computed from ocean surface gravity waves as measured by the bow-mounted acoustic altimeter array and the polarimetric camera, defined from long gravity waves to pure capillary waves. Used for estimation of Stokes drift profile. Shaded region represents the 5^{th}-95^{th} percentile range. Dashed line shows the k^{-3} slope in log-log space.

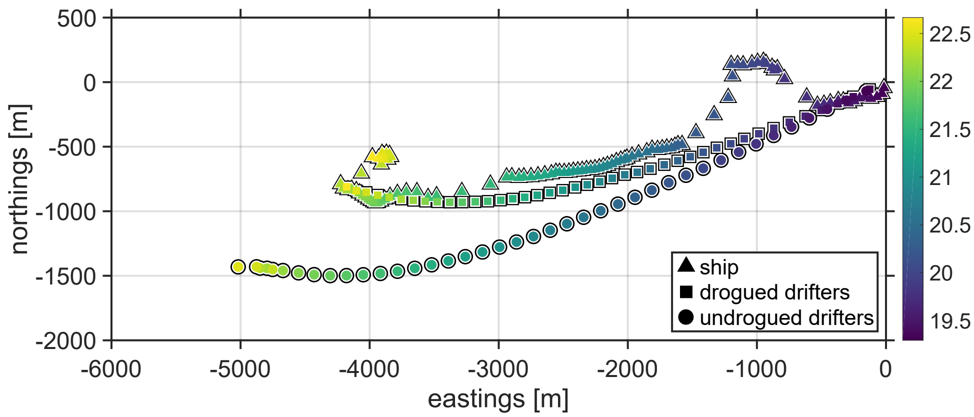

Figure 4. Trajectories of ship (triangles), drogued drifter centroid (squares), and undrogued drifter centroid (circles) during observation time. Origin of local coordinate system is deployment location. Colorbar indicates the hour (UTC) of April 27th, 2017.